Title: Polymers with Controlled Assembly and Rigidity Made with Click-functional Peptide Bundles

Authors: Dongdong Wu[1], Nairiti Sinha[1], Jeeyoung Lee[1], Bryan Sutherland[1], Nicole Halaszynski[1], Yu Tian[1], Jeffrey Caplan[2], Huixi Violet Zhang[3], Jeffery G. Saven[3,*], Christopher J. Kloxin[1,4,*], and Darrin J. Pochan[1,*]

Affiliations:

1) Department of Materials Science and Engineering, University of Delaware, Newark, DE 19716
2) Delaware Biotechnology Institute, University of Delaware, Newark, DE 19711
3) Department of Chemistry, University of Pennsylvania, Philadelphia PA, 19104
4) Department of Chemical and Biological Engineering, University of Delaware, Newark, DE 19716

*** Corresponding authors:** pochan@udel.edu, cjk@udel.edu, saven@upenn.edu

The engineering of biological molecules for materials applications is a foundational concept in the design of highly functional, sophisticated soft matter. Biomolecules present a wide range of structures and functions: chemical recognition (e.g. enzyme substrates or adhesive ligand display*(1)* exquisite nanostructures using peptides(*2*), proteins(*3*), or nucleic acids(*4*); and unique mechanical properties including silk-like strength(*3*), biocomposite stiffness(*5*), viscoelasticity(*6*), and resiliency(*7*). Herein, computational peptide design of physical (noncovalent) interactions is combined with pathway-dependent, hierarchical covalent assembly to produce hybrid synthetic polymers. The fundamental monomer units of these polymers are homotetrametic, alpha-helical peptide bundles. These bundle monomers, or 'bundlemers', can be designed to provide complete control of stability, size, and spatial display of chemical functionality. The protein-like structure of the bundle allows regioselective positioning of covalent linkages between the peptide termini in distinct bundlemers resulting in polymers that exhibit a variety of interesting and controllable physical characteristics, including the formation of stiff rigid-rods, semiflexible and kinked chains, and thermally responsive hydrogel networks. Such polymeric assemblies are achieved using a small molecular weight peptide. By using designed peptide bundles as nanometer-scale monomer building blocks, targeted polymer chain properties have been decoupled from subtleties and limitations associated with using small molecular weight monomers in a polymer synthesis. Furthermore, with control of the amino acid sequence along the bundlemer periphery, specific side chains can be used to conjugate moieties in a desired pattern, opening possibilities to create a wide variety of hybrid nanomaterials.

The bundlemer polymer chains exhibit a variety of unique features. In contrast with high molecular weight synthetic polymers, the chains employ small (~3 kD), easily synthesized peptide sequences that fold/assemble into designed tetrameric 4 nm bundles. The subsequent covalent assembly yields polymers with micron-scale contour lengths. The design of alpha-helical homo-oligomers has a long history using both empirical de novo*(8)* and computational*(9)* methods. Herein, homotetrameric bundles with D_2 symmetry*(10)* present two reactive groups at each end via chemical functionalization of the constituent peptide N-terminus (**Figure 1A**). Chemically distinct homotetrameric bundles wtih complementary reactive functional groups are chemically linked to produce bundlemer chains.

The first example of a bundlemer chain uses two different coiled coil peptide bundles*(10)* with complementary reactive groups for covalent polymerization (**Figure 1A)**. One peptide (Peptide 1, **Figure ED1**) contains a maleimide functionality at the N-terminus, resulting in two maleimides at each end of the folded bundlemer. The second peptide contains cysteine as the N-terminal amino acid (Peptide 2, **Figure ED1**). The maleimide and thiol groups undergo a thiol-Michael addition reaction (**Figure ED2**) to produce two covalent bonds between neighboring bundlemers producing a hybrid polymer chain maintained by both the covalent linkages and the complementary, noncovalent (physical) interactions within each bundlemer. The resultant polymers exhibit an unprecedented rigid-rod character. Both negatively stained transmission electron microscopy (TEM) and cryogenic TEM (cryoTEM) data reveal extreme chain stiffness (**Figures 1B-D**). Direct imaging of the rigid-rods is possible since the polymer cross-section is defined by

77 constituent bundlemers. Small-angle neutron scattering (SANS) of the rigid-rod polymers
78 confirmed that the cross-sections are, in fact, a single bundlemer in diameter ~2 nm **(Figure**
79 **ED3)**. While 1-D assemblies of proteins can exhibit a high rigidity (e.g., viruses(*11, 12*),
80 actin(*13,14*) , microtubulin(*13*), mis-folded globular proteins(*15*)), all are assemblies of
81 much larger proteins with many interparticle interactions, much wider cross-sections, and
82 significant ratios of protein molecular mass to linear length of the rod(*16*). Similarly, past
83 physically assembled coiled coils(*17-19*) produced stiff fibers with large cross-sections
84 relative to the protein or peptide building blocks. Fibrils rich in β-sheet consisting of
85 misfolded proteins, such as bovine serum albumin*(20,21)* or β-lactoglobulin*(22)*, as well
86 as short, de novo designed peptides*(23)*, exhibit large persistence lengths spanning 10 nm
87 for thinner fibrils up to approximately 10 μm for thicker fibrils. However, the stiffer,
88 thicker β-sheet fibrils have significant mass per length to produce such high persistence
89 length 1-D nanostructure. The biopolymer with the closest cross-section to what is
90 observed here is double stranded DNA; however, DNA has a persistence length, l_p, of $l_p \leq$
91 50 nm, depending on solution conditions.(*24*) The TEM and cryoTEM data in **Figure 1**
92 show rods greater than 1 μm in length that display rigid-rod behavior along the entire chain
93 length. Estimates of the rod persistence length based on methods developed for rod and
94 fiber analysis in two dimensions(*21*) provide values of $l_p > 30$ μm (**Figure ED4)**,
95 highlighting the extraordinary stiffness for such a thin, molecular object. For perspective,
96 the persistence length vs. mass per unit length of the bundlemer rigid rods is plotted in
97 **Figure ED5** relative to other peptide or protein 1-D polymeric nanostructures discussed
98 above.
99

Hybrid physical-covalent chains using proteins have until now produced flexible chains due to the flexibility of linear polymer linkers(*25*) or dimeric coiled coils(*26*) that link the final polymer together. Hexameric peptide coiled coils have produced semiflexible nanotube chains through electrostatic interactions(*27*) or native chemical ligation; these semiflexible nanotubes exhibited an irregular chain trajectory and were shorter than the rigid-rods produced herein. An important aspect of bundlemer chain rigidity is the use of antiparallel homotetrameric bundlemers as the building block for polymerization. Formation of both possible covalent linkages is highly likely (**Figure 1A**) since once a covalent bond between partner bundlemers forms, formation of the second cross-link between the same pair is expected to be more likely than a linkage to a third bundle. The thiol and maleimide reaction sites are closely displayed from the end of the rigid bundlemer, and the dual linkage between adjacent bundlemers further restricts conformational flexibility within the final rigid rod chain. This designed crosslinking is in contrast to linkages among the parallel, hexameric coiled coils where defects in linking produce semiflexible chains with possible branch points (*27*). The design of two covalent linkages between adjacent peptide bundles with D_2 symmetry minimizes chain defects and provides extreme polymer rigidity.

The efficiency of the thiol-Michael reaction allows targeting of rigid-rod length through simple reactant stoichiometric control. The ultralong (micron) rigid-rods in **Figure 1B,1C** were synthesized with a 1:1 ratio of bundlemers displaying thiol and maleimide (Peptide 2 : Peptide 1). Through simple alteration of the relative bundle ratio **(**10:9, see **Methods)**, much shorter rigid rods can be produced **(Figure 1D).**

Just as one is not limited to a single bundlemer building block or polymer length, one also can use different organic interbundle linkers to alter physical chain characteristics while still producing a targeted bundlemer pattern along the chain. For example, maleimide functionalized bundles (Peptide 1) reacting with the organic tetrathiol, pentaerythritol tetrakis(3-mercaptopropionate) (PETMP, **Figure ED6**), produce a semiflexible chain (**Figure 1E)**. The chain flexibility is due solely to the molecular flexibility of the PETMP since the same maleimide-functionalized bundlemer was used to make rigid-rod chains. SANS of the semiflexible chains in solution indicates a chain cross-section equal to that of one peptide bundle, as observed with the rigid-rods **(Figure ED3)**. One can combine rigid-rod and semiflexible segments within a single polymer. Short, rigid-rods with maleimide-functionalized bundlemerss at the rod termini subsequently can be reacted with PETMP to produce kinked, segmented chains **(Figure 1F)**, with the kinks due to the PETMP conformational flexibility. Importantly, various polymer architectures and flexibilities are possible using the same bundlemer building blocks, thereby separating the characteristics of the chain contour from the designed amino acid sequence.

The hybrid physical-covalent peptide rods exhibit lyotropic liquid crystalline (LC) behavior in concentrated solution with optical textures typical of lamellar phases. Toric focal conic domains (TFCDs) are observed in smectic LCs when confined to thin films in which the smectic layers are generally parallel with the sample substrate**.(***28*) Apparent TFCDs are observed in polarizing optical microscopy of concentrated rod solution thin films **(Figure 2)**. Peptide or protein fibrillar assemblies are known to form LC phases due

146 to inherent rod-like character.(*29*) Given the extreme stiffness of these new physical-
147 covalent bundlemer rods, the ability to target desired rod length distributions, and the
148 ability to alter rod chemistry using computational design and non-natural amino acids,
149 these systems provide opportunities in new LC material design.
150
151 Locally within the rigid rods, one purposefully can display and pattern chemical moieties,
152 ranging from small molecule dyes to synthetic polymers to inorganic nanoparticles. Super-
153 resolution fluorescence microscopy(*30*) provides the tool for observation of rigid-rods
154 synthesized with fluorophores attached to specific lysine side chains. Rods with targeted
155 lengths of ~50 nm were first assembled **(Figure 1)** with the short rod termini consisting of
156 bundlemers displaying thiols **(Figure 3A,** more description in **Methods)**. These short rods
157 were functionalized with either a green (Peptide 3) or red (Peptide 4) fluorescent dye (5(6)-
158 carboxy-tetramethylrhodamine, green; 4-chloro-7-nitrobenzofurazan, red; see **Figure 3A**).
159 Separate populations of short red rods and short green rods were mixed together along with
160 unlabeled bundles with maleimide termini (**Figure 1A** and **Figure 3A**) in order to link the
161 short, dye-labeled rods together into longer rigid-rods. Stochastic optical reconstruction
162 microscopy (STORM)*(30)* allows clear observation of the ~50 nm long, individual red or
163 green rod segments within longer rods (**Figure 3A**).
164
165 Bundlemers within the rigid-rod chains can denature at high temperature, resulting in
166 bundlemer chain disassembly, but can reversibly reform rigid rods below the bundlemer
167 melting temperature. In the case of the rigid-rods in **Figure 3**, when the temperature was
168 increased to 90°C all constituent bundles denatured, causing the rigid-rods to fall apart into

169 covalently linked dimers of peptides, each containing one dye-labeled peptide and one
170 peptide without dye (**Figure 3B)**. On lowering the temperature to 25 C, the bundlemers
171 re-assemble and, consequently, physically re-polymerize into rigid-rods. However, the
172 dyes that were originally segregated into ~50 nm red or green segments within the longer
173 rigid-rods are now mixed along the entire length of the reformed rigid-rods, **Figure 3C**.
174 This is a direct effect of the assembly pathway. The segregation of dyes within the rods
175 created in the original pathway was erased with temperature to create a similar rigid-rod
176 superstructure but with the original dye segmentation now scrambled.
177
178 The use of high molecular weight organic reagents to link bundlemers together *(6)* yields
179 thermally responsive hydrogels. Maleimide-bearing bundlemers coupled to a 20 kD
180 tetrathiol having four poly(ethylene glycol) arms (**Figure ED6**) act as crosslinking points
181 in a hybrid bundlemer-PEG hydrogel network. The choice of the bundlemer as hydrogel
182 crosslinker can be used to control the network temperature response. The maleimide-
183 terminated Peptide 1 bundlemer, which has a melting temperature of T_m = 55°C *(10)* was
184 used as the network crosslinking junction. The hydrogel can be reversibly disassembled
185 and reformed through cycling temperature above and below the bundlemer melting
186 temperature (**Figure ED7**). In contrast, use of the Peptide 5 bundlemer (T_m = 80°C) *(10)*
187 produces a network that is robust to much higher temperatures (**Figure ED7)**.
188
189 The structure of the bundlemer polymer can be leveraged to pattern additional, orthogonal
190 click reactions. Peptide 6 (**ED1**) contains a lysine at residue 13 that is functionalized to
191 present an alkyne (**SI Scheme S5,)** that can react with an azide to form a triazole linkage

192 via the CuAAC reaction (copper(I)-catalyzed azide–alkyne cycloaddition). Bundlemer
193 rods built using Peptide 6 were functionalized with azide-terminated polyethylene glycol
194 polymers (PEG_{2000}). AFM studies (**Figure 4**) display height variation along the
195 longitudinal rod axes having a peak spacing of approximately 10 nm (**Figure 4D**),
196 consistent with the expected spacing of the PEG-functionalized bundles within the rigid
197 rod.
198
199 While engineered click reactions can be used to link desired moieties to precise locations
200 along the bundlemer chains, the noncovalent self-assembly of the bundlemers themselves
201 also has the potential to order moieties that are conjugated to the peptide chains *prior* to
202 bundlemer formation. Peptide 7 (**Figure ED1**) was designed to display a thiol group only
203 at residue 24 and conjugated with maleimide-functionalized gold nanoparticles (**Figure 4**).
204 Subsequent aqueous assembly produces a dominant nanostructure of gold nanoparticle
205 chains with a sub 5 nm interparticle spacing consistent with interspacing of bundlemers
206 between adjacent nanoparticles. The hybrid gold nanoparticle-bundlemer chains exhibit
207 changes in apparent distance between gold nanoparticles and changes in the chain
208 trajectory due to the multiple possibilities of gold particle-bundlemer connection.
209
210 The tools of computational design for coiled coil building blocks combined with
211 engineered covalent interactions provide new possibilities for physical-covalent
212 programmable polymers, for peptide liquid crystalline materials, and even for one-, two-
213 and three-dimensional nanostructures. The ‘bundlemer’ concept also imparts potential
214 functionality to these structures made possible with natural and non-natural amino acids.

Overall, bundlemers provide a simple, versatile toolbox for a wide range of materials design and refinement all while harnessing the design possibilities and function afforded by biologically inspired peptide molecules.

References:

1 Lutolf, M.P., Hubbell, J.A. Synthetic biomaterials as instructive extracellular microenvironments for morphogenesis in tissue engineering. *Nature Biotechnology*, **23**, 47–55 (2005).

2 Egelman, E. H., Xu, C., DiMaio, F., Magnotti, E., Modlin, C., Yu, X., Wright, E., Baker, D., Conticello, V. P. Structural Plasticity of Helical Nanotubes Based on Coiled-Coil Assemblies. *Structure* **23**, 280-289, (2015).

3 Yang, Y. J., Holmberg, A. L. & Olsen, B. D. Artificially Engineered Protein Polymers. *Annual Review of Chemical and Biomolecular Engineering,* Vol. 8 (ed J. M. Prausnitz) 549-575 (2017).

4 Seeman, N. C. & Sleiman, H. F. DNA nanotechnology. *Nature Reviews Materials* **3**, Article number: 17068 (2018).

5 Ding, Z.Z., Ma, J., He, W., Ge, Z.L., Lu, Z.Q., Kaplan, D.L. Simulation of ECM with silk and chitosan nanocomposite materials. *Journal of Materials Chemistry B* **5**, 4789-4796 (2017).

6 Dooling, L. J., Buck, M. E., Zhang, W.-B. & Tirrell, D. A. Programming Molecular Association and Viscoelastic Behavior in Protein Networks. *Advanced materials (Weinheim)* **28**, 4651-4657, (2016).

239 7 Li, L. Q., Tong, Z. X., Jia, X. Q. & Kiick, K. L. Resilin-like polypeptide hydrogels
240 engineered for versatile biological function. *Soft Matter* **9**, 665-673, (2013).
241 8 Bryson, J.W., Betz, S.F., Lu, H.S., Suich, D.J., Zhou, H., O'Neil K.T., DeGrado,
242 W.F. Protein Design - a Hierarchical Approach. *Science*. **270,** 935–41 (1995).
243 9 Huang, P-S, Oberdorfer, G., Xu, C., Pei, X.Y., Nannenga, B.L., Rogers, J.M.,
244 DiMaio. F., Gonen, T., Luisi, B., Baker, D. High thermodynamic stability of
245 parametrically designed helical bundles. *Science*. American Association for the
246 Advancement of *Science*, **346**, 481–485 (2014).
247 10 Zhang, H.V., Polzer, F., Haider, M.J., Tian, Y., Villegas, J.A., Kiick, K.L., Pochan,
248 D.J. & Saven, J.G. Computationally designed peptides for self-assembly of
249 nanostructured lattices. *Science Advances* **2**, article e1600307 (2016).
250 11 Dogic, Z. & Fraden, S. Ordered phases of filamentous viruses. *Current Opinion in*
251 *Colloid and Interface Science* **11**, 47-55, (2006).
252 12 Dogic, Z. Surface freezing and a two-step pathway of the isotropic-smectic phase
253 transition in colloidal rods. *Physical Review Letters* **91,** article 165701 (2003).
254 13 Gittes, F., Mickey, B., Nettleton, J. & Howard, J. Flexural Rigidity Of Microtubules
255 And Actin-Filaments Measured From Thermal Fluctuations In Shape. *Journal of*
256 *Cell Biology* **120**, 923-934, (1993).
257 14 Zhang, R., Kumar, N., Ross, J. L., Gardel, M. L. & de Pablo, J. J. Interplay of
258 structure, elasticity, and dynamics in actin-based nematic materials. *Proceedings of*
259 *the National Academy of Sciences of the United States of America* **115**, E124-E133,
260 (2018).

15 Zhao, J. G., Bolisetty, S., Adamcik, J., Han, J., Fernandez-Ronco, M.P. & Mezzenga, R. Freeze-Thaw Cycling Induced Isotropic-Nematic Coexistence of Amyloid Fibrils Suspensions. *Langmuir* **32**, 2492-2499, (2016).

16 Bharti, B., Fameau, A. L., Rubinstein, M. & Velev, O. D. Nanocapillarity-mediated magnetic assembly of nanoparticles into ultraflexible filaments and reconfigurable networks. *Nature Materials* **14**, 1104-1109, (2015).

17 Hume, J., Sun, J., Jacquet, R., Renfrew, P.D., Martin, J.A., Bonneau, R., Gilchrist, M.L. & Montclare, J.K. Engineered Coiled-Coil Protein Microfibers. *Biomacromolecules* **15**, 3503-3510 (2014).

18 Papapostolou, D., Smith, A.M., Atkins, E.D.T., Oliver, S.J., Ryadnov, M.J., Serpell, L.C. & Woolfson, D.N. Engineering nanoscale order into a designed protein fiber. *Proceedings of the National Academy of Sciences of the United States of America* **104**, 10853-10858, (2007).

19 Dong, H., Paramonov, S. E. & Hartgerink, J. D. Self-assembly of alpha-helical coiled coil nanofibers. *Journal of the American Chemical Society* **130**, 13691-13695, (2008).

20 Usov, I., Adamcik, J., Mezzenga, R. Polymorphism Complexity and Handedness Inversion in Serum Albumin Amyloid Fibrils, *ACS Nano*, **7**, 10465−10474 (2013).

21 Usov, I.; Mezzenga, R. FiberApp: An Open-Source Software for Tracking and Analyzing Polymers, Filaments, Biomacromolecules, and Fibrous Objects, *Macromolecules*, **48**, 1269-1280 (2015).

22 VandenAkker, C.C.; Engel, M.F.M.; Velikov, K.P.; Bonn, M.; Koenderink, G.H. Morphology and Persistence Length of Amyloid Fibrils Are Correlated to Peptide Molecular Structure. *J. Am. Chem. Soc.*, **133**, 18030–18033 (2011).

23 Aggeli, A.; Nyrkova, I.A.; Bell, M.; Harding, R.; Carrick, L.; McLeish, T.C.B.; Semenov, A.N.; Boden, N. Hierarchical Self-Assembly of Chiral Rod-like Molecules as a Model for Peptide β-Sheet Tapes, Ribbons, Fibrils, and Fibers, *Proceedings of the National Academy of Sciences of the United States of America*, **98**, 11857-11862 (2001).

24 Manning, G. S. The persistence length of DNA is reached from the persistence length of its null isomer through an internal electrostatic stretching force. *Biophysical Journal* **91**, 3607-3616, (2006).

25 Averick, S., Karacsony, O., Mohin, J., Yong, X., Moellers, N.M., Woodman, B.F., Zhu, W.P., Mehl, R.A., Balazs, A.C., Kowalewski, T. & Matyjaszewski, K. Cooperative, Reversible Self-Assembly of Covalently Pre-Linked Proteins into Giant Fibrous Structures. *Angewandte Chemie-International Edition* **53**, 8050-8055, (2014).

26 Oshaben, K. M. & Horne, W. S. Tuning Assembly Size in Peptide-Based Supramolecular Polymers by Modulation of Subunit Association Affinity. *Biomacromolecules* **15**, 1436-1442, (2014).

27 Thomas, F., Burgess, N. C., Thomson, A. R. & Woolfson, D. N. Controlling the Assembly of Coiled-Coil Peptide Nanotubes. *Angewandte Chemie-International Edition* **55**, 987-991, (2016).

28 Ok, J. M., Kim, H., Jeong, H.S., Yoo, H.W., Kim, J.H., Srinivasarao, M., Jung, H.T. Control of periodic defect arrays of 8CB (4 '-n-octyl-4-cyano-biphenyl) liquid crystals by multi-directional rubbing. *Soft Matter* **9**, 10135-10140, (2013).

29 Dogic, Z. Filamentous Phages As a Model System in Soft Matter Physics. *Frontiers in Microbiology* **7**, 1013 (2016).

30 Huang, B., Bates, M., Zhuang, X. Super-resolution Fluorescence Microscopy. *Annu. Rev. Biochem.* **78***,* 993–1016 (2009).

Acknowledgements: Funding was provided by the Department of Energy, Office of Basic Energy Sciences, Biomolecular Materials Program under grant Nos. DE-SC0019355 and DE-SC0019282. Funding also was provided under cooperative agreement 70NANB12H239 and 70NANB17H302 from NIST, U.S. Department of Commerce. DJP and NS also acknowledge the support of the National Institute of Standards and Technology, U.S. Department of Commerce, in providing the neutron research facilities used in this work. Neutron facilities are also supported in part by the National Science Foundation under Agreement No. DMR-0944772. The National Institutes of Health (RO1 EB006006) are acknowledged for support and the UD COBRE NIH-COBRE 1P30. GM110758 and 1P20 RR017716 are acknowledged for instrument resources. The Delaware INBRE grant no. P20 GM103446 is acknowledged for support of the Delaware Biotechnology Institute. J.G.S. acknowledges partial support from the Penn Laboratory for Research on the Structure of Matter (MRSEC, NSF DMR-1120901) and NSF CHE-1709518. The statements, findings, conclusions and recommendations are those of the authors and do not necessarily reflect the view of NIST, the U.S. Department of Commerce,

or the U.D. Department of Energy. DW, DJP, CJK acknowledge internal research support from the University of Delaware.

Authors Contributions: DJP, CJK, and JGS conceived of the project and mentored research activity as well as contributed to the writing of the manuscript. DW performed peptide synthesis, AuNP synthesis and peptide conjugation with subsequent assembly into AuNP-bundle chains, bundle and bundlemer polymer formation and characterization, and contributed to the writing of the manuscript. JL and NS contributed to the characterization via TEM, cryoTEM, POM, and SANS with NS contributing to the writing of the manuscript. BS and NH performed peptide synthesis, molecular characterization, rod formation, and PEG conjugation. YT performed AFM characterization. JC performed the STORM characterization and contributed to the writing of the manuscript. HVZ performed the computational design and modeling of peptides.

Competing Interests: The authors have no financial or non-financial competing interests with respect to the manuscript.

Materials and Correspondance: All requests should be made to Darrin Pochan (pochan@udel.edu) or Christopher Kloxin (cjk@udel.edu) or Jeffery Saven (saven@upenn.edu).

Figure Captions

Figure 1: Peptides designed for homotetrameric, antiparallel coiled-coil formation *(25)* with polymer formation upon covalent assembly. **A)** At N-termini (blue), Peptide 1 and Peptide 2 (**Figure ED1**) have maleimide (Mal) and cysteine (C), respectively; C-terminus (red) of each peptide is unreactive. Each sequence forms homotetrameric bundlemers: Peptide 1 (grey cylinder); Peptide 2 (white cylinder). Thiol-maleimide click reaction yields chains with two covalent linkages between neighboring bundlemers. **B)** TEM of rigid-rods produced using 1:1 ratio of Peptides 1 and 2. Sample negatively stained with phosphotungstic acid (PTA). **C)** CryoTEM of rigid rod in aqueous solution with length > 1 micron. **D)** Negatively stained TEM of short rigid rod chains produced using asymmetric ratio (10:9) of reacting bundlemers. **E)** PETMP organic tetrathiol links Peptide 1 bundlemers to form semiflexible chains. **F)** Segmented chains produced by connecting short rigid rods with PETMP. Rod segments within the segmented polymer range in length from approximately 50 nm (n is approximately 3 to 4) to 100 nm (n is approximately 8 to 9).

Figure 2: Liquid crystal (LC) behavior of concentrated rigid rod solutions. Rods prepared as in Figure 1A, 1D with alternating bundlemerss of Peptide 1 and Peptide 2. **A)** Polarized optical microscopy (POM) of a pseudoisotropic region of ~100 nm long rods with multiple toric focal conic domains (TFCDs) indicative of a lyotropic lamellar phase. POM was performed on an 8 w/v % short rigid-rod solution at pH 2. **B)** TEM of negatively stained short rigid rods from pseudoisotropic region shown in A, with clear rod layering. **C)** TEM reveals structure from dilute regions in which rigid-rods have locally aggregated into

droplets with clear rod orientation. **D)** Schematic of a TFCD cross-section formed in smectic A-type LC. Enlarged schematic (red) of a single smectic layer showing the proposed homeotropic alignment of individual rigid-rods. The blue dashed lines represent boundaries between smectic layers confined between parallel walls (thick black lines, the glass slide and cover slip in the POM, respectively). LC director **n** in the film is perpendicular to the smectic layers. Local orientation director (gray arrows) within the smectic A layers is parallel to **n** far from the TFCD. In the vicinity of topological defect (yellow), the local orientation field folds towards the defect.

Figure 3: Reversible noncovalent assembly of rod polymers. **A)** Rigid rods were created using fluorescently labeled variants (Peptide 3 and 4, **Figure ED1**), each containing either 4-chloro-7-nitrobenzofurazan (green) or 5(6)-carboxy-tetramethylrhodamine (red) attached to the K24 side chain. Bundlemers of Peptide 2 (white) are used in formation of short rigid-rods comprising a single dye type. Resulting red and green rods are joined via Peptide 1 bundles (gray) to make longer rods with red and green segments. STORM images are of resulting longer rigid-rods. Each segment's constituent red or green fluorescence is easily resolved. **B)** Rigid rods from (A) are heated to T = 90 °C, above the constituent bundle melting temperatures, resulting in unfolding and dissociation of the individual bundles while peptide dimers remain covalently linked. On cooling the solution to T = 20 °C, below the melting temperature of the coiled coils, the bundlemers and rigid-rods reform. **C)** Reassembled rods now display co-localization of green and red fluorescence (yellow signal when the green and red channels are displayed concurrently) along the entire reformed rod lengths.

Figure 4: Bundle display of non-natural side chains affords templated, patterned display of polymers from rigid rod bundlemers or assembly of hybrid metal nanoparticle-bundle chains. **A)** Atomic Force Microscopy (AFM) image of rigid rods formed using Peptide 2 and Peptide 6 (**Figure ED1**), with azide-functionalized PEG_{2000} chains conjugated to the rigid rods. **B)** AFM image of rigid rod-area within green rectangle used for height analysis along rod longitudinal axis. **C)** Schematic illustrating bundles of Peptide 6 (gray) and Peptide 2 (white) and conjugated PEG_{2000}. **D)** Height trace along longitudinal axis indicated in B. **E)** Maleimide-functionalized gold nanoparticles are conjugated with Peptide 7 (**Figure ED1**). Peptide 7 is subsequently allowed to assemble producing hybrid nanoparticle-bundlemer chains. E) TEM of nanoparticle-bundlemer chains. F) TEM of nanoparticle-bundlemer chains reveals interparticle separation consistent with dimensions of peptide bundles.

Methods:

Synthetic schemes and details for all synthetic amino acids, peptides, and functionalized gold nanoparticles are described in detail in the Supplemental Information.

Experimental details for preparing different bundlemer polymers using covalent thiol-maleimide reaction.

Rigid rods: Two separate solutions, one of Peptide 1 (**Figure ED1**) and one of Peptide 2 (**Figure ED1**), were prepared, each with 1 mM peptide in phosphate buffer (pH 6, 25 mM), for the respective formation of each homomeric bundle. Then, the two bundle solutions

were mixed with the same volumes, and 0.2 eq. tris(2- carboxyethyl)phosphine (TCEP, 50 mM in DI water) was added as catalyst. The bundle mixture was shaken overnight at room temperature to produce the rods. **Alkyne-containing rods:** To make rods of Peptide 6 and Peptide 2 (**Figure ED1**) for PEG conjugation, 1 μmol of each peptide as freshly lyophilized powder was added to a 2 mL Eppendorf tube. To the solid mixture, 200 μL of Millipore H_2O was added to make a 5 mM solution of bundles, and the solution was vortexed. The pH of the system was checked (pH ~6). The solution was mixed at room temperature for 12 h and at 60 °C for an additional 12 h.

Representative maleimide-excessive short rigid rods: Two peptide solutions of Peptide 1 and Peptide 2 in phosphate buffer (pH 6, 25 mM) were prepared at 1 w/v %, respectively. The two bundle solutions with different volumes were mixed to achieve the molar ratio of maleimide/thiol = 10/9 (e.g., mix 0.528 mL solution Peptide 1 and 0.472 mL solution of Peptide 2 to make 1mL 1 w/v% solution). Then, TCEP (50 mM in DI water) at 0.2 eq. relative to peptide 2 was added as catalyst. The mixture was shaken overnight at room temperature to produce the short rigid rods.

Semi-flexible chains: Separate solutions of 1 mM Peptide 1 and 0.25 mM pentaerythritol tetrakis(3-mercaptopropionate) (PETMP, **Figure ED6**) were each prepared in phosphate buffer (pH 6, 25 mM). PETMP was purchased from *Sigma*. The same volumes of the two solutions were mixed, and 0.2 eq. of TCEP (50 mM in DI water) relative to Peptide 1 was added as catalyst. The mixture was shaken overnight at room temperature to produce the semi-flexible chains.

Procedure to make kinked chains: 1 mL of 1 w/v% short rigid rod solution (with an excess of maleimide-containg bundles to guarantee maleimide termini of the short rods, molar ratio of maleimide to thiol is 10 to 9) was prepared with the protocol described earlier. PETMP (2.9 µL, 50 mM) was added to make the ratio maleimide/thiol = 1. The mixture was shaken at room temperature for a week to produce kinked chains.

Procedure to conjugate azide-functionalized PEG to alkyne-functionalized rods with Cu-catalyzed click reaction: Stock solutions in Millipore H_2O were prepared of $CuSO_4$ (200 mM), tris-hydroxypropyltriazolylmethylamine (THPTA) (400 mM), and sodium ascorbate (1 M). To a 1.5 mL Eppendorf tube was added 40 µL of 5 mM peptide, which had previously been assembled into rods. Then N_3-PEG_{2000} (2 mg, 5eq) was dissolved in 160 µL of Millipore water and added to the peptide rod solution. From the respective stock solutions was added 1 µL $CuSO_4$ (2 eq), 1 µL of THPTA (4 eq), and 2 µL of sodium ascorbate (10 eq). The solution was purged with nitrogen then vortexed and mixed at 40 °C for 48 h.

Procedure to conjugate maleimide-functionalized AuNPs to thiol-functionalized Peptide 7 with subsequent AuNP-Peptide 7 bundle chain formation:

1 mg of gold nanoparticles functionalized with maleimide groups (AuNPs-Mal, SI Scheme 7) was dissolved in 1 mL dimethyl formamide (DMF) to make a transparent yellow solution. 5 µL of DMF solution consisting of 1 mM thiol-functionalized Peptide 7 (**Figure ED1**) and 0.2 eq. TCEP was added to the AuNPs-Mal DMF solution. The mixture was

reacted overnight at room temperature to produce the AuNPs conjugated with Peptide 7. Then the solution was dialyzed against pure water to afford coiled coil bundle formation by the conjugated Peptide 7 in order to produce AuNP-Peptide 7 bundle chains.

Representative 3 w/v% hydrogel of Peptide 1 with 4-arm PEG tetra-thiol (20K Da): 8 mg Peptide **1** and 10.86 mg 4-arm PEG tetra-thiol (20K Da) were dissolved in 620 μL phosphate buffer (pH 6, 25 mM). 0.2 eq. TCEP (9 μL, 50 mM in DI water) relative to Peptide **1** was added as catalyst. The mixture was shaken at room temperature. The hydrogel usually formed after 2 to 4 hours of reaction. 4-arm PEG tetra-thiol (20K Da) was purchased from *JenKem Technology*.

Transmission Electron Microscopy (TEM): Carbon-coated 200 mesh copper grids (CF200-Cu, Electron Microscopy Sciences, Inc.) were freshly treated by glow discharge using a plasma cleaner (PDC-32G, Harrica Plasma, Inc.) at low level for 20 seconds. Then, 4 μL sample solution was dropped on the grid. After 1 min, the remaining liquid was blotted from the edge of the grid using filter paper. The grid was allowed to air-dry for 10 min before TEM observation on FEI TALOS™ F200C microscope. For negative staining, 6 μL aqueous solution of phosphotungstic acid (2 w/v%, pH 6) was applied to the dried grid and incubated for 15-30 seconds. Then the grid was blotted with filter paper. The stained grid was allowed to sit for 10 min before TEM observation.

The cryogenic-TEM imaging was also performed on FEI TALOS™ F200C microscope with the accelerating voltage at 200 kV. Lacey grids from Ted Pella, Inc. were used for all grid preparation after the oxygen plasma treatment. Vitrified grid preparation

for cryo-TEM was done by using the Vitrobot™, an automated plunge freezing device that vitrifies a thin solution layer to liquid N_2 temperature. A sample droplet of 1.5 μL was deposited to the plasma cleaned lacey grids. Depending on sample viscosity and concentration, blotting parameters were adjusted to obtain the most optimal liquid film thickness, usually requiring 2-3 blottings lasting 1-2 s at 100 % humidity. After blotting, the sample grids were allowed 2 seconds for relaxation. In order to achieve extremely fast cooling rate for homogenous vitreous layer, the grid was plunged into liquid ethane (~ -175°C) and then transferred to LN_2 for storage. During the imaging, the cryo-TEM holder was maintained at -177°C to prevent ice crystallization or sublimation. The images were recorded with either FEI Ceta 16M (CCD) or Falcon-II camera (CMOS) at a low electron dose.

Small angle neutron scattering (SANS): SANS experiments were performed on the NG-B 30 m SANS instrument, a part of the Center for High Resolution Neutron Scattering (CHRNS) at the National Center for Neutron Research (NCNR), National Institute of Standards and Technology, Gaithersburg, MD. Installed on a 60 mm x 60 mm split neutron guide NG-B, this instrument delivers a neutron beam of wavelength (λ) of ≈ 6 Å with a resolution ($\Delta\lambda / \lambda$) of 10 % at full width at half maximum (FWHM). The detector installed on this instrument is a 640 mm x 640 mm ^{3}He position-sensitive counter with a resolution of 5.08 mm x 5.08 mm. Sample-to-detector lengths of 1 m, 4 m and 13 m were employed to cover a q-range of 0.0035 $Å^{-1}$ to 0.4 $Å^{-1}$ for scattering experiments involving the 1 w/v % semi-flexible chains. A wider q-range of 0.0015 $Å^{-1}$ to 0.35 $Å^{-1}$ was covered for scattering experiments on 1 w/v % rigid rods, enabled by the additional use of neutron lenses at the 13 m detector configuration. Here, q is the scattering vector given by $q =$

$4\pi \sin(\theta/2)/\lambda$. The raw data obtained from scattering experiments was corrected for background noise and radiation, detector sensitivity, and open beam transmission using IgorPro*(31)* software to obtain a normalized scattering intensity curve. Standard deviation was calculated statistically using the number of averaged detector counts at each data point. The reduced 1D scattering intensity obtained after buffer subtraction was fitted to various models using SasView*(32)* software.

Scattering from an isotropic solution of non-interacting, monodisperse species is described by the general equation*(33)*:

$$I(q) = nV^2(\Delta\rho)^2 P(q)$$

Here, $I(q)$ is the normalized scattered intensity as a function of scattering vector q; n is the number density of scattering species; V is the volume of each scatterer; $\Delta\rho$ is the difference in scattering length density (SLD) between the scattering species and solvent; and P(q) is the form factor, given by the average geometric shape of the scattering species in solution.

For fitting the scattering curve from rigid rod solution in SasView, a cylinder model was chosen, the P(q) of which is calculated by(*34,35)*:

$$P(q) = \frac{\text{scale}}{V}\int_0^{\pi/2} f^2(q,\alpha)\sin\alpha\, d\alpha + \text{background}$$

where,

$$f(q,\alpha) = 2(\Delta\rho)V * \frac{\sin\left(qL\cos\frac{\alpha}{2}\right)}{qL\cos\frac{\alpha}{2}} * \frac{J_1(qr\sin\alpha)}{qr\sin\alpha}$$

Here, J_1 is the first order Bessel function; α is the angle between the cylinder axis and the scattering vector q; L is the length of the cylinder; r is its radius. An integral over α from 0

to $\pi/2$ radians averages the scattering intensity over all possible orientations of rods in an isotropic solution.

For semi-flexible rods, a flexible cylinder model fit was performed in SasView. Its form factor P(q) is defined by the equation*(31,33,34)*:

$$P(q) = \frac{\text{scale}}{V}\langle f(q,\alpha)\rangle^2 + \text{bkg}$$

where $\langle f(q,\alpha)\rangle^2$ is a squared average scattering over all possible orientations α for a given scattering vector q. A worm-like semi-flexible cylindrical chain is used having a contour length L, radius r and Kuhn length $K_b = 2\ l_p$, where l_p being the persistence length of the worm-like chain. This model also incorporates excluded volume interactions between segments of the worm-like chain in solution.

Optical Microscopy: A 15 w/v % solution of short rigid rods of average length ~200 nm was prepared by gently concentrating a dilute solution of rods as described in the paper by Jung and Mezzenga*(36)*. Nitrogen gas was blown at a low flow rate into a flask containing 0.5 w/v % solution of short rigid rods that was kept under constant, mild agitation. This slowly concentrated the solution by evaporating water molecules from the exposed air-water interface, avoiding the formation of non-equilibrium structures such as crystalline aggregates during the concentration process. The concentrated solution was then adjusted to pH 2 by adding a few drops of 1 N hydrochloric acid. Anhydrous sodium chloride was added to yield a rod solution containing ~100 mM salt. Samples for polarized optical microscopy were prepared by adding 2 μL of the solution between clean glass slide and cover slip. The freshly prepared sample slides were immediately investigated for birefringence due to formation of liquid crystalline phases under polarized light in

transmission mode on an Olympus BX60 Light Microscope at 20 °C. High-resolution images were captured by a Nikon DS-Fi1 digital camera and the images were analyzed using NIS-Elements imaging software.

Rheological measurement: The hydrogels were prepared as the protocol described below. The measurement was performed on a TA Instruments DHR-3 rheometer (TA Instruments, New Castle, DE). The hydrogel was deposited (160 μL) onto the rheometer stage. A 20 mm stainless-steel parallel plate was used and the gap height was set as 500 μm for measurement. Oil was applied to seal the sample. The storage modulus G′ and loss modulus G″ were monitored under an applied strain of 0.01% to 10000% at a frequency of 1 rad/s for the strain sweep, and a frequency of 0.1 rad/s to 200 rad/s at strain 0.1% for frequency sweep. Temperature sweeps were performed at the range of 25 °C to 80 °C at 5 degree increments. Temperature reversible experiments were carried out by subjecting the gel to 0.5% strain and 1 rad/s frequency.

Experimental details for STORM micrographs on super resolution microscopy

Solution sample preparation for rigid rods with individual rod segments containing either red or green dye: Two 0.5 mL peptide solutions of short rigid rods with thiol termini were prepared from click reactions between identical volumes of Peptides **2** (1 mM) and **3** (0.9 mM) (**Figure ED1**) and between the identical volumes of Peptides **2** (1 mM) with **4** (0.9 mM) (**Figure ED1**). Each of the two short, rigid rod solutions then were mixed with an identical volume having the appropriate amount of Peptide **1** (100 μL, 1 mM) to make the ratio of total added maleimide group to thiol end groups equal to 1:1 in

the entire solution. The mixture was shaken at room temperature for a week to produce longer chains containing short rod segments of red or green dye.

Solution sample preparation of temperature denatured and subsequently re-assembled rigid rods with mixed red and green dye along entire rod length: The solution of rigid rods with red and green dye-containing segments was heated to 90 °C for 10 minutes to denature the rigid rods. The solution then was incubated at 4 °C for 24 hours to reassemble the constituent bundles resulting in rigid rods with green and red dye mixed along the entire length of the rods.

STORM imaging: The STORM images were taken on the Zeiss Elyra PS.1 super-resolution microscope. Rods were mounted on a high-precision 22 mm x 22 mm coverslip (Zeiss) by applying a 10 μL rod solution for 10 seconds. The remaining liquid was removed using filter paper. The sample adhered to the coverslip was rinsed with phosphate buffer (pH 6, 25 mM) 5 times. An oxygen scavenging buffer (540 mM glucose, 3.1 μM Catalase, 7.6 μM Glucose Oxidase, 10 mM NaCl, 20 mM Cysteamine) in 58 mM TRIS-HCl was added on the sample just before image acquisition and sealed in a magnetic CF chamber (Chamlide). STORM images with 4-chloro-7-nitrobenzofurazan and 5(6)-carboxy-tetramethylrhodamine were taken with a Plan-Apochromat 100x/1.46 oil objective with 488 and 561 nm laser excitation, respectively. For each STORM image, 500 frames were acquired, aligned using a model-based algorithm, and filtered with 1 - 30 nm precision. For STORM imaging of rigid rods with individual rod segments containing either red or green dye, images were taken sequentially, merged, and then aligned. All image processing steps were completed in the Zen 2012 software.

Atomic Force Microscopy (AFM): AFM was performed on a Bruker Multimode system using Bruker ScanAsyst Air ultra-sharp tips with a nominal tip radius of 2 nm and a spring constant of 0.4 N m^{-1}. Freshly cleaved mica discs (Ted Pella, Inc.) were used as substrates for sample deposition. Samples were prepared by spin-coating 20 μL of ~5 mM PEG_{2000}-conjugated bundlemer rod sample solution onto a freshly cleaved mica disc using a spin-coater (WS-650SZ, Laurel Technologies). The spin-coater was set to 500 rpm for 10s at the first stage, during which, the sample solution was pipetted onto the substrate. Then the speed was sequentially increased to 2000 rpm and held for 3 min at the second stage to spin off the liquid. During the 3 min of spin coating, 20 μL of Milli-Q water was applied to wash off excess salts. The mica disc appeared to be dry after the spin-coating and then was rested for at least 1 hour before subject to AFM imaging. The instrument was operated in peak force tapping mode. A new AFM tip was used for each different sample. Peak force set-point was manually adjusted to optimize the spatial resolution as well as to minimize the sample damage. Scanning was performed in the horizontal direction and repeated in the 45˚ diagonal direction to exclude scanning artifacts. Micrographs were recorded digitally using Bruker Nanoscope software with 512 lines at a 0.5 Hz scan rate and corrected for background undulations using in-software algorism function.

Data Availability Statement: The authors declare that the data supporting the findings of this study are available within the paper and its supplementary information files. Additional, ray data are available from the corresponding author upon reasonable request.

627 Methods and Extended Data References:

628 31 Kline, S.R. Reduction and analysis of SANS and USANS data using IGOR Pro. *J.*
629 *Appl. Crystallogr.* **39,** 895–900 (2006).

630 32. SasView, http://www.sasview.org

631 33. Guinier, A. & Fournet, G. Small-angle scattering of X-rays. (John Wiley and Sons,
632 Inc., 1955).

633 34. Pedersen, J.S. & Schurtenberger, P. Scattering Functions of Semiflexible Polymers
634 with and without Excluded Volume Effects. *Macromolecules* **29**, 7602–7612
635 (1996).

636 35. Chen, W., Butler, P.D. & Magid, L.J. Incorporating Intermicellar Interactions in
637 the Fitting of SANS Data from Cationic Wormlike Micelles. *Langmuir* **22**, 6539–
638 6548 (2006).

639 36. Jung, J. & Mezzenga, R. Liquid Crystalline Phase Behavior of Protein Fibers in
640 Water: Experiments versus Theory. **26**, 504–514 (2010)

641 37. Haider, M.J., Zhang, H., Sinha, N., Saven, J.G., Pochan, D.J. Self-assembly and
642 soluble aggregate behavior of computationally designed coiled-coil peptide
643 bundles, *Soft Matter*, **14**, 5488-5496 (2018).

644 38. Kas, J., Strey, H., Sackmann, E. Direct Imaging of Reptation for Semiflexible Actin
645 Filaments. *Nature*, **368**, 226−229 (1994).

646 39. Boal, D.H. *Mechanics of the Cell,* Cambridge University Press, 2012 (calculated
647 persistence length using measurements of TMV flexural rigidity in Falvo, et al.,
648 *Biophysical Journal, 72*, 1396-1403 (1997)).

649

Extended Data Figure Captions

ED1. Structures of peptides 1-7 used in this work. Structures of the chemical modifications to the terminal amine (Mal) and to lysine side chains are presented. The unmodified amino acid sequences of Peptide 1, Peptide 2 (without N-terminal Cys), and Peptide 6 have been previously denoted P622_6 *(10)*, BNDL1 *(10)*, and BNDL2 *(37)*, respectively.

ED2. Thiol-maleimide click reaction.

ED3. Small-angle neutron scattering (SANS) of peptide rods with different linker chemistry. (A) Scattering from rigid rods [□] and the corresponding rigid cylinder fit [▬]. Rigid rods (identical long rods as discussed in Figure 1B) were assembled in 25 mM pH 6 phosphate buffer prepared in deuterated water at 20°C. (B) Scattering from semi-flexible fibers [Δ] and the corresponding flexible cylinder fit [▬]. Semi-flexible chains (identical chains as shown in Figure 1E) were dissolved in 25 mM pH 6 phosphate buffer prepared in deuterated water at 20 °C. (C) Polymer radii fit results of the SANS scattering data using form factor models in SasView.*(32)*

ED4. Estimation of persistence length of rigid rod bundle chains using FiberApp tracking and analysis software package from Usov and Mezzenga.*(21)* A) CryoTEM of rigid rod bundle chains. B) Same rigid rod bundle chains after software tracking. C) Plot of calculated mean-squared end-to-end distance (MSED) between contour segments along the tracked rod (□) and corresponding fit MSED fit (▬) between contour segments based on the worm-like chain model in two-dimensions with the following theoretical dependence: $\langle R^2 \rangle = 4\lambda[l - 2\lambda(1 - e^{-l/2\lambda})]$, where λ is the persistence length and R is the direct distance between any pair of segments along a contour separated by an arc length l. Persistence length is estimated to be 33.4 +/- 0.4 μm. D) Alternate method for persistence length estimation for very stiff, one-dimensional objects is the mean-squared midpoint displacement (MSMD). Plot of calculated MSMD between contour segments along the tracked rod (□) and corresponding MSMD fit (▬) based on the equation that describes the behavior of a midpoint deviation along a rod $\langle u_x^2 \rangle = l^3/48\lambda$, where $\langle u_x^2 \rangle$ is the mean-squared midpoint displacement between any pair of segments along a tracked rod contour,

separated by an arc length l, assuming the displacements are small in comparison to the corresponding arc lengths ($|u_x| \ll l$). This method estimates the rod persistence length to be 41.3 +/- 0.5 μm.

ED5. Plot of persistence length vs. mass per unit length of various 1-D polymers and molecular assemblies (adapted from Bharti).*(16)* Values of persistence length for the various 1-D polymers and assemblies determined from or taken from the following references: Peptide bundlemer rigid rod chains estimated from cryoTEM data herein based on methods of Usov and Mezzenga *(21),* Hydrocarbon polymers *(16)*, Fd and M13 viruses *(11,12)*, DNA *(16,24)*, F-actin *(13,38)*, Tobacco Mosaic Virus *(16,39)*, microtubulin *(13,39)*, thin (2-3 nm in diameter) and thick (4-6 nm in diameter) twisted bovine serum albumin (BSA) fibers *(20)*, β-lactoglobulin, β-sheet rich, twisted fibrils that range in diameter from 1-6 nm with a mean diameter ~3 nm *(22)*, 11 amino acid, β-sheet ribbons with low stacking (producing ribbon diameters ~4 nm in diameter) and high stacking (producing ribbons with diameters ranging from 4-8 nm) *(23)*.

ED6. Chemical structures of bundlemer organic linkers. Structure of pentaerythritol tetrakis(3-mercaptopropionate) (PETMP) for semi-flexible chain or kinked chain formation. Chemical structure of 4-arm PEG tetra-thiol (20K Da) for hydrogel formation.

ED7. Hydrogel network rheology. Hydrogels comprised of Peptides 1 and 5 (**Figure ED1**) linked with 20 kD 4-arm PEG tetra-thiol (**Figure ED6)**. Temperature dependence of loss and storage moduli as functions of temperature (left) and upon cycling temperature,

where temperature ramps were performed over 5 minutes in between 2 minute-long isothermal measurements (right). **A)** Peptide 1 with T_m = 55 °C. Peptide 1 exhibits a temperature reversible hydrogel due to the low melting temperature of the designed peptide. **B)** Peptide 5 with T_m = 85 °C. The hydrogel produced with a Peptide 5 is stable to approximately 85 °C and shows much more rigid gel properties at all temperatures observed.

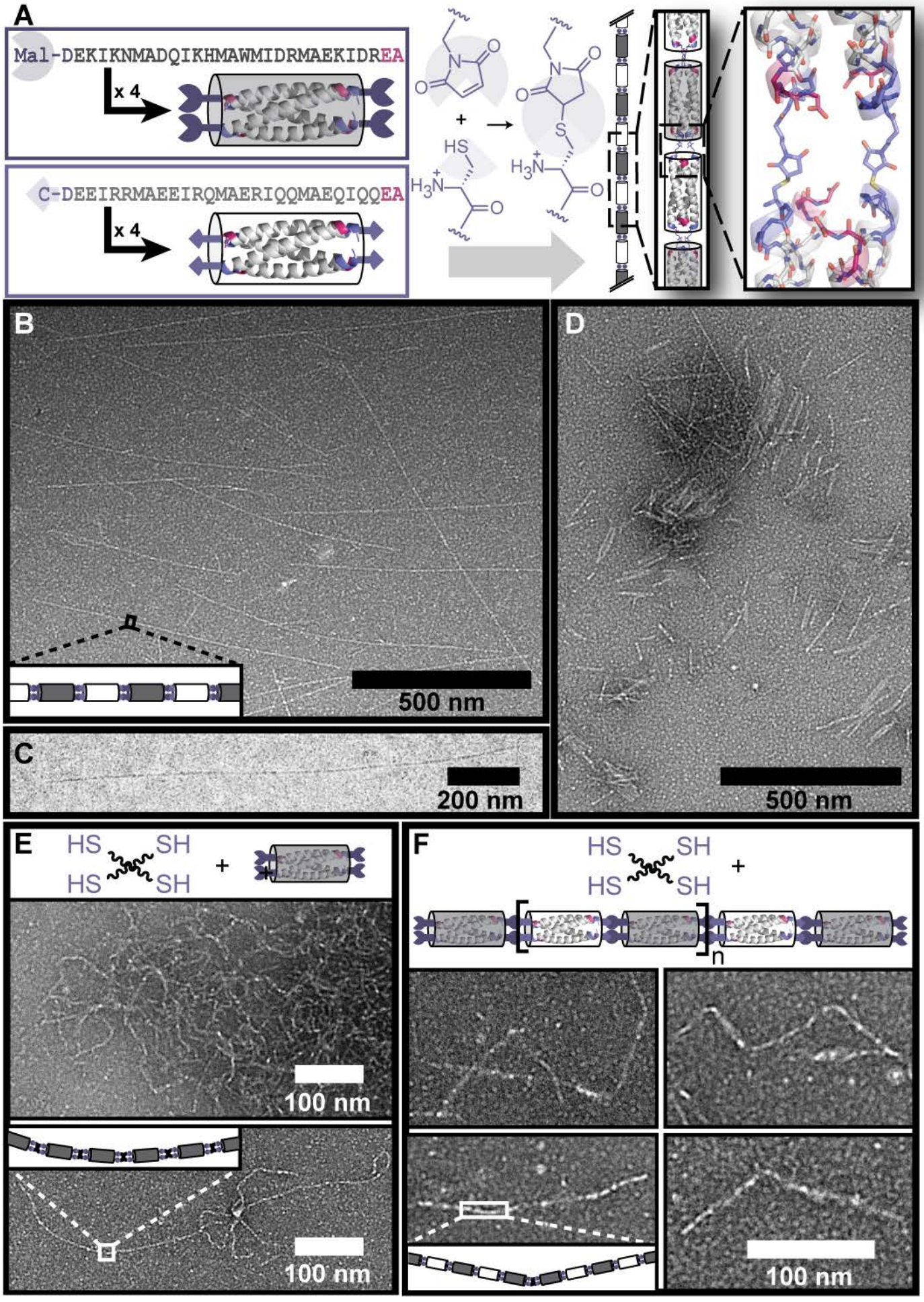
A
Mal-DEKIKNMADQIKHMAWMIDRMAEKIDREA
x 4
C-DEEIRRMAEEIRQMAERIQQMAEQIQQEA
x 4
B
500 nm
C
200 nm
D
500 nm
E
HS SH
HS SH
100 nm
100 nm
F
HS SH
HS SH
n
100 nm

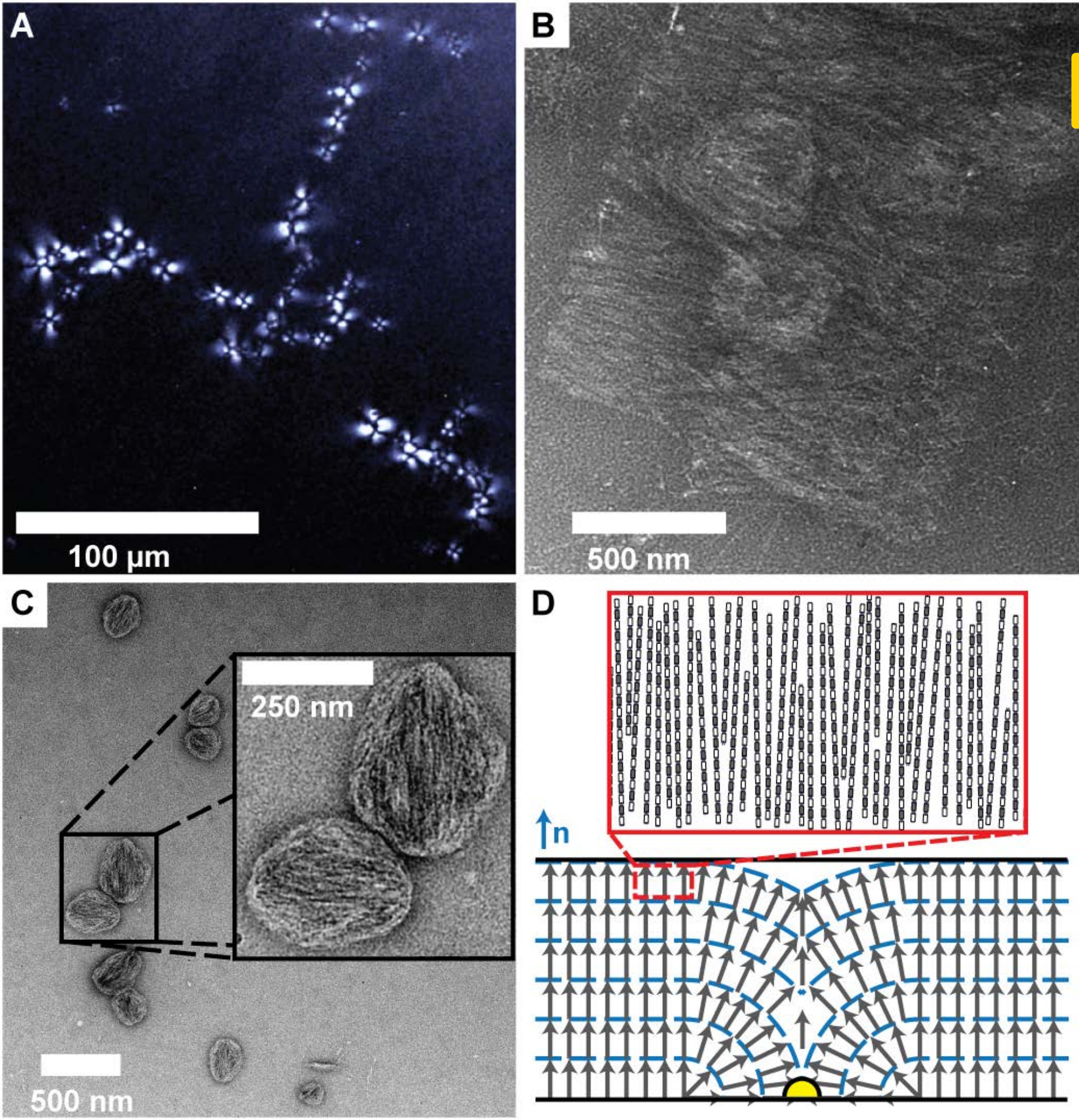
A
100 µm
B
500 nm
C
250 nm
500 nm
D
n

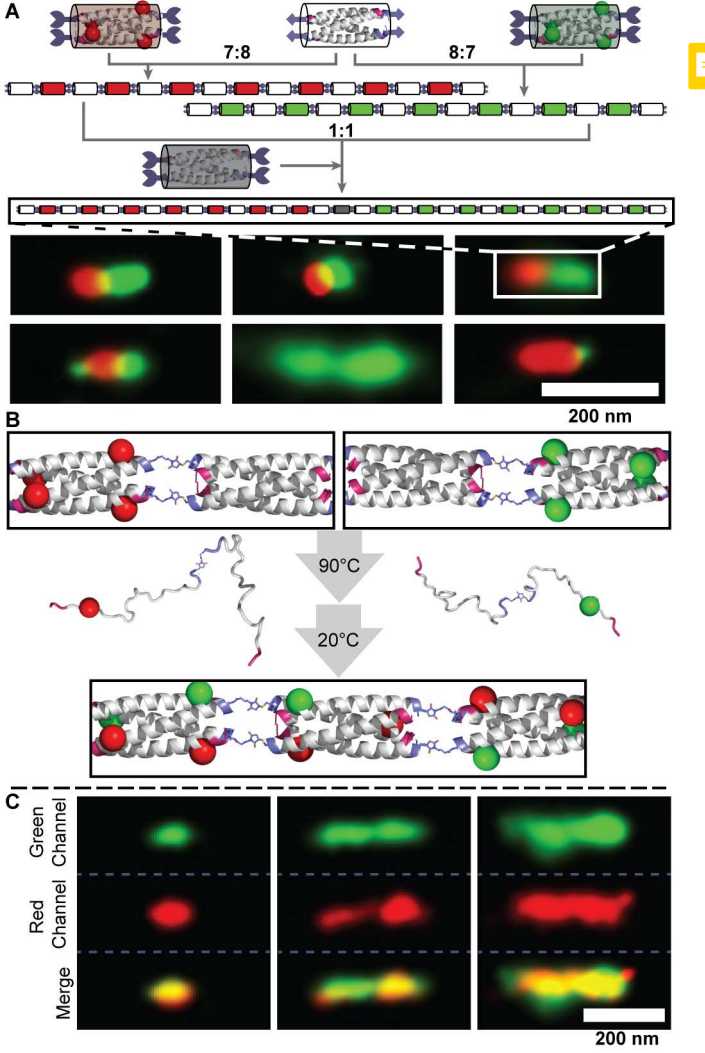
A
7:8
8:7
1:1
200 nm
B
90°C
20°C
C
Green Channel
Red Channel
Merge
200 nm

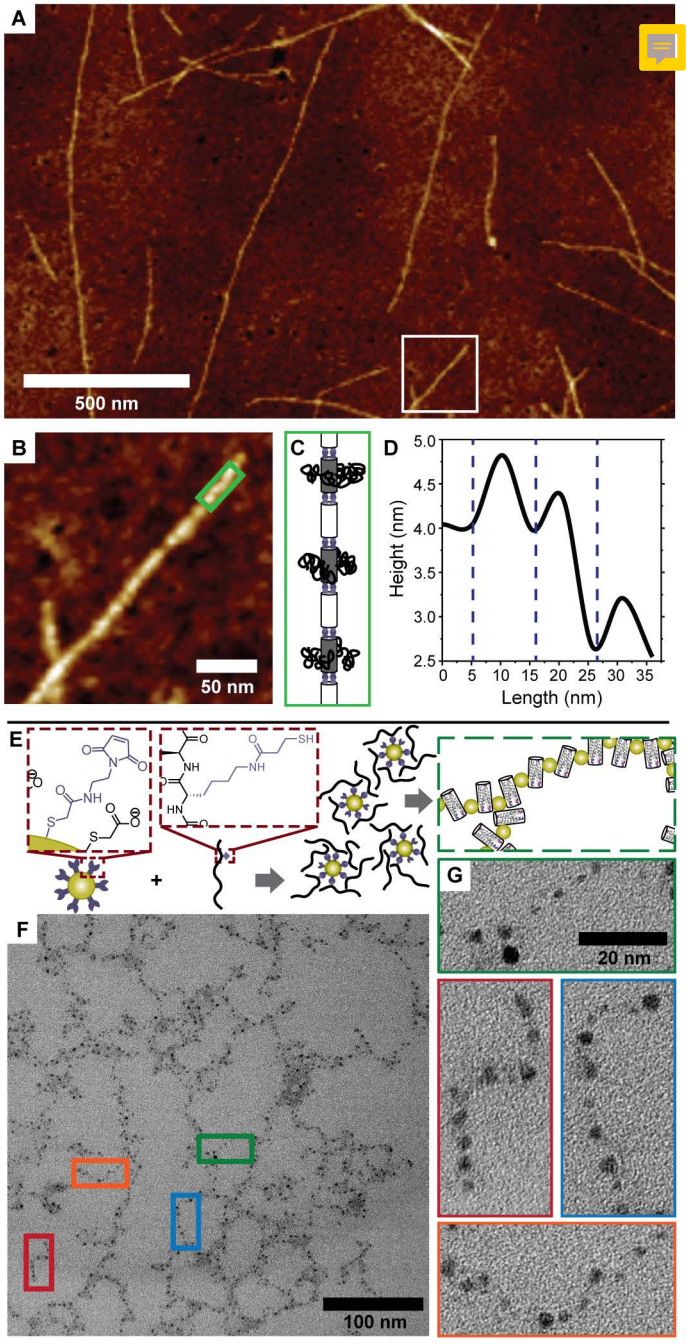
A
500 nm
B
50 nm
C
D
Height (nm)
Length (nm)
E
SH
NH
HN
+
G
20 nm
F
100 nm

Peptide	Sequence
	N *C*
1	**Mal**-DEKIKNM ADQIKHM AWMIDRM AEKIDRE A
2	C-DEEIRRM AEEIRQM AERIQQM AEQIQQE A
3	**Mal**-DEKIKNM ADQIKHM AWMIDRM AE**K**IDRE A
4	**Mal**-DEKIKNM ADQIKHM AWMIDRM AE**K**IDRE A
5	**Mal**-REEIRRM AEEIRRM AREIERM AEEIERR A
6	**Mal**-DEKIKNM ADQIK**K**M AWMIDRM AEKIDRE A
7	DEKIKNM ADQIKHM AWMIDRM AE**K**IDRE A

Mal

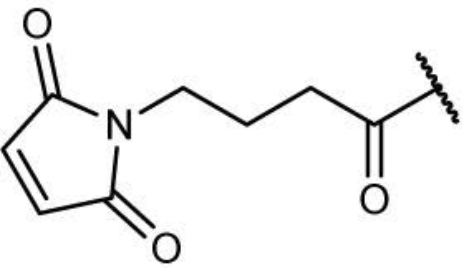

K

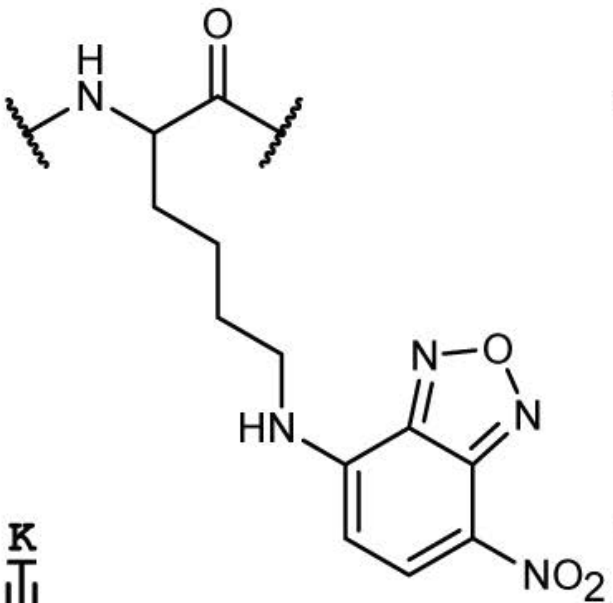

K

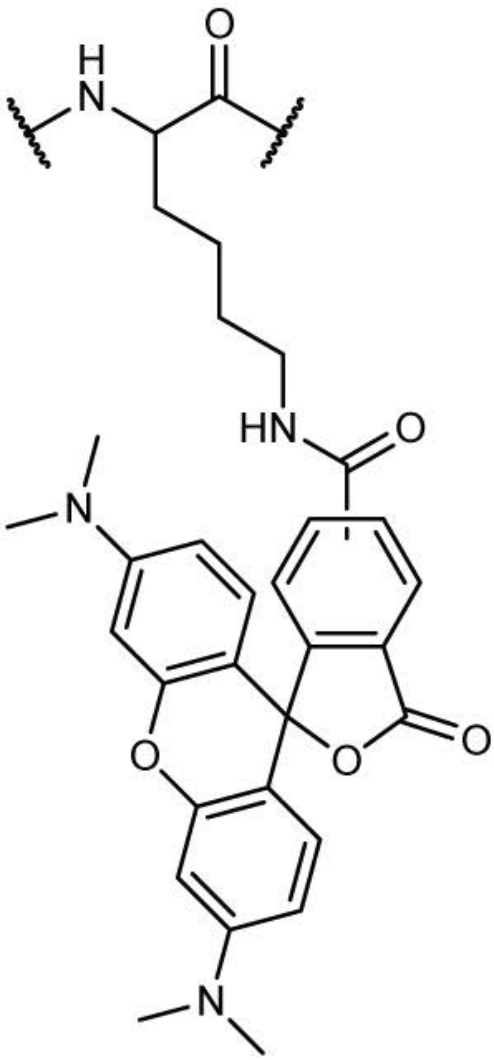

K
SH

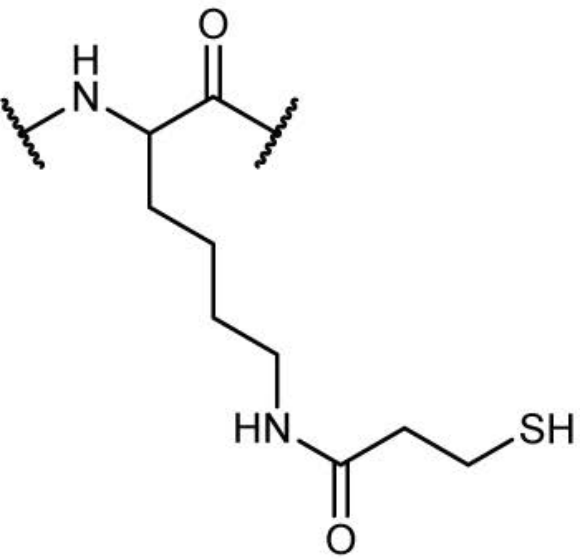

K

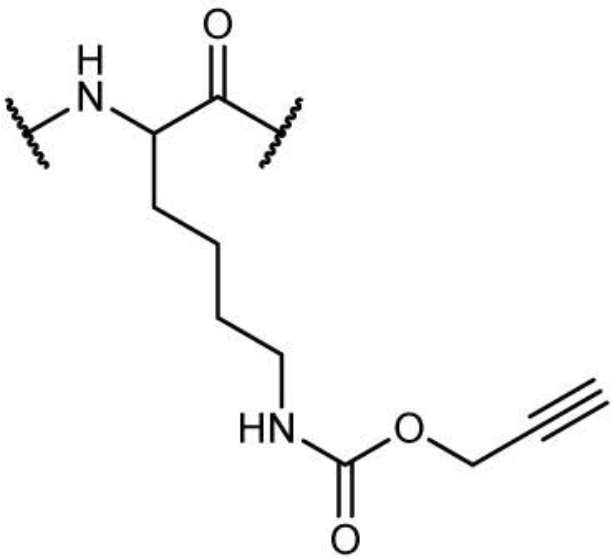

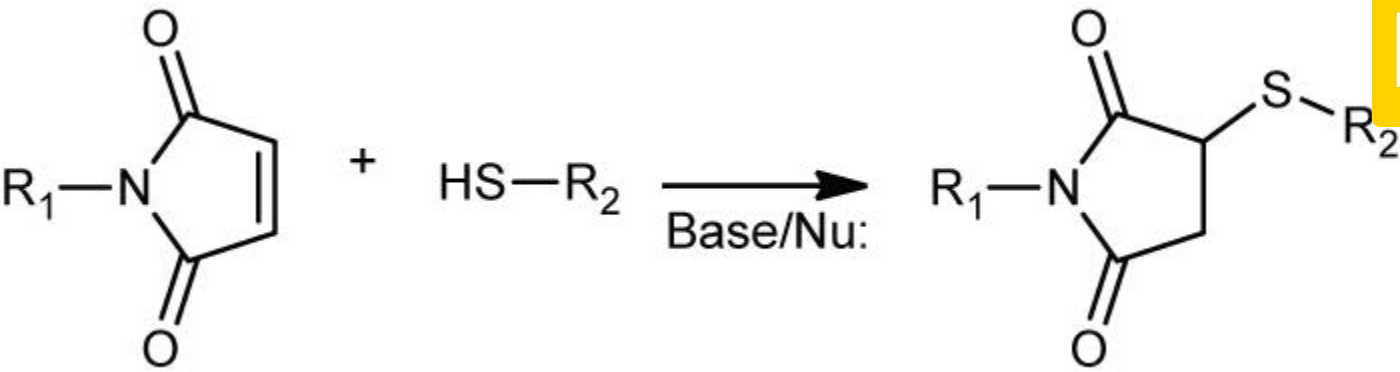
O
R1—N
O
+
HS—R2
Base/Nu:
O
S
R2
R1—N
O

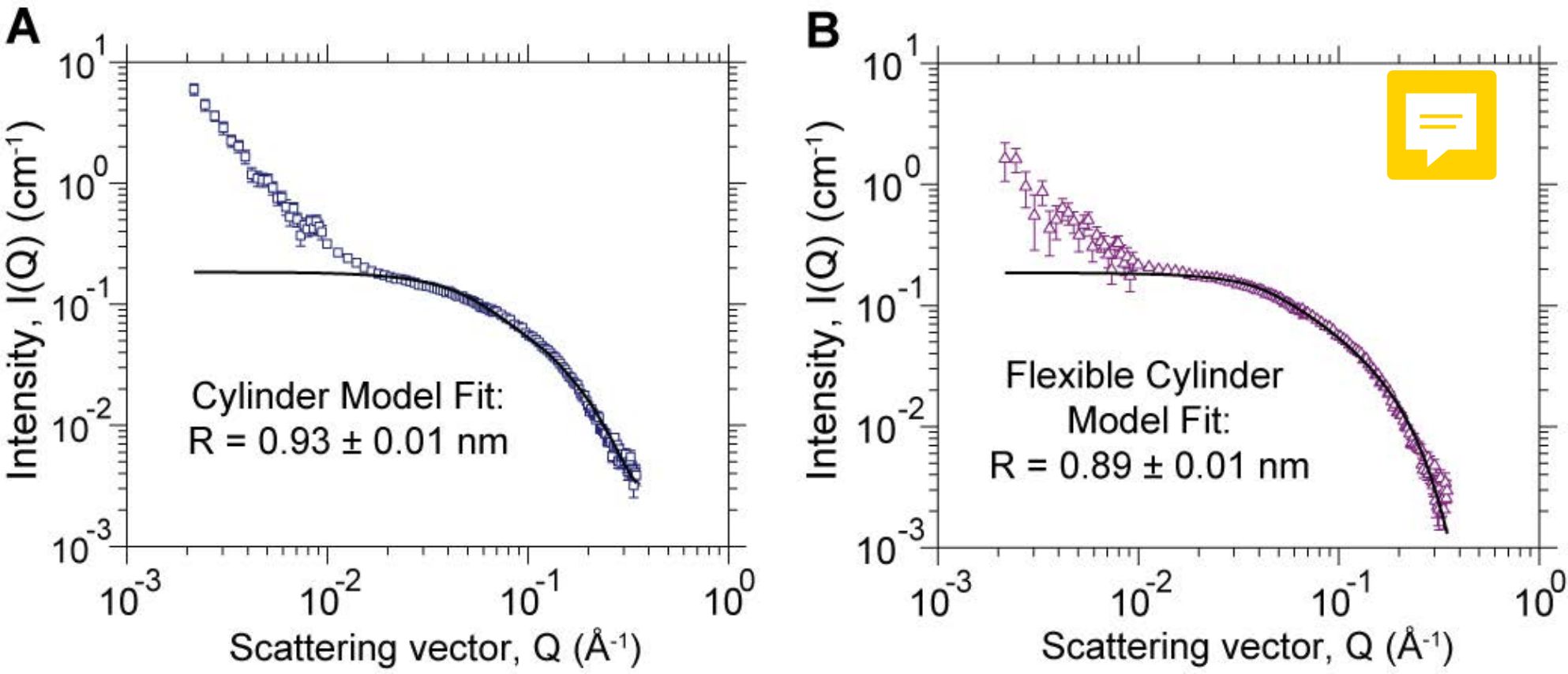
A
Intensity, I(Q) (cm-1)
Scattering vector, Q (Å-1)
Cylinder Model Fit:
R = 0.93 ± 0.01 nm
B
Intensity, I(Q) (cm-1)
Scattering vector, Q (Å-1)
Flexible Cylinder
Model Fit:
R = 0.89 ± 0.01 nm

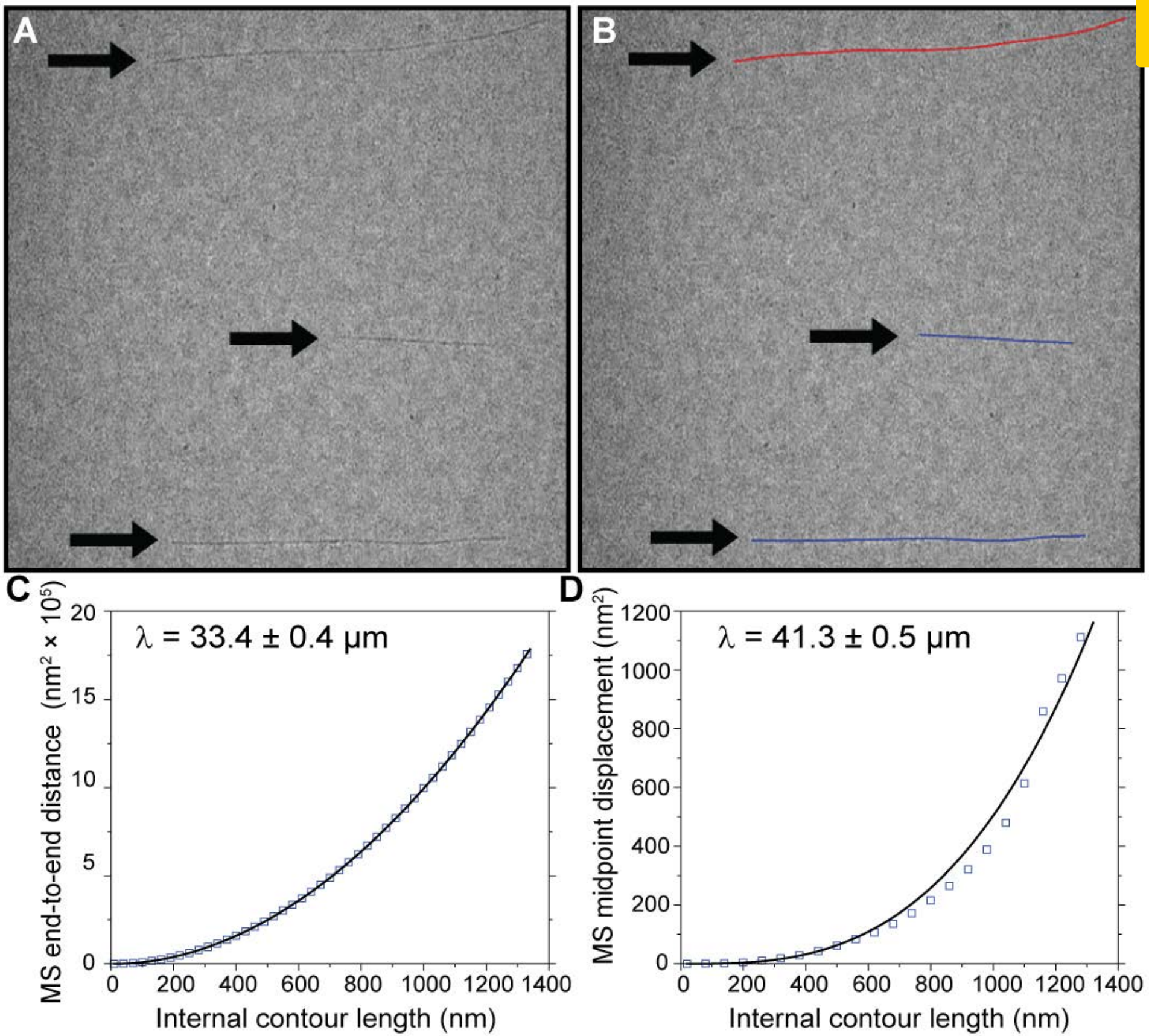
A
B
C
λ = 33.4 ± 0.4 μm
MS end-to-end distance (nm² × 10⁵)
0
5
10
15
20
0
200
400
600
800
1000
1200
1400
Internal contour length (nm)
D
λ = 41.3 ± 0.5 μm
MS midpoint displacement (nm²)
0
200
400
600
800
1000
1200
0
200
400
600
800
1000
1200
1400
Internal contour length (nm)

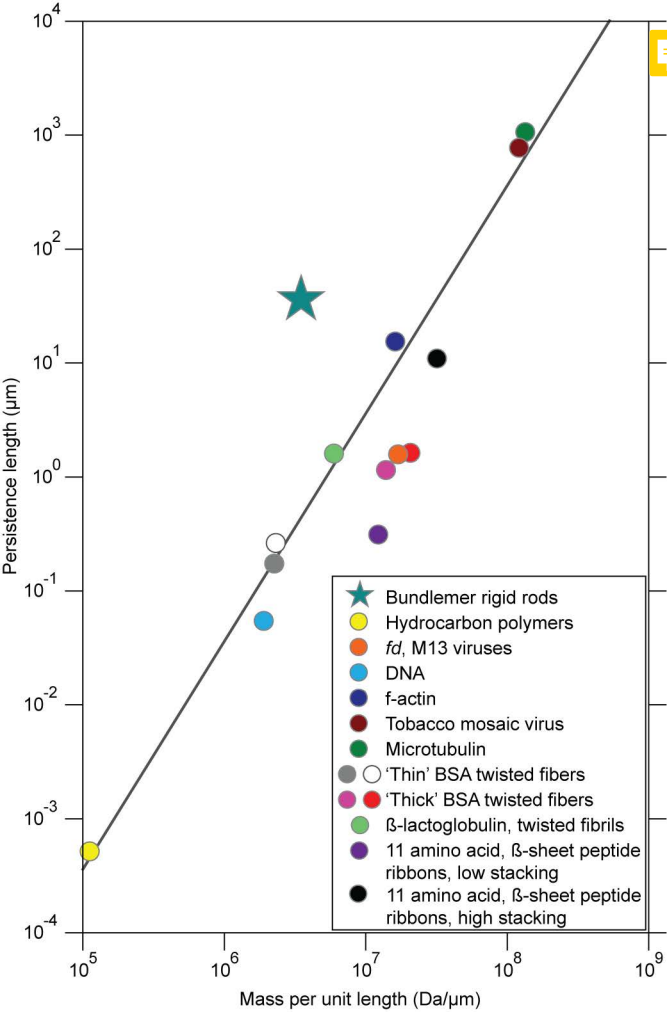
Persistence length (μm)
Mass per unit length (Da/μm)
Bundlemer rigid rods
Hydrocarbon polymers
fd, M13 viruses
DNA
f-actin
Tobacco mosaic virus
Microtubulin
'Thin' BSA twisted fibers
'Thick' BSA twisted fibers
ß-lactoglobulin, twisted fibrils
11 amino acid, ß-sheet peptide ribbons, low stacking
11 amino acid, ß-sheet peptide ribbons, high stacking

A)

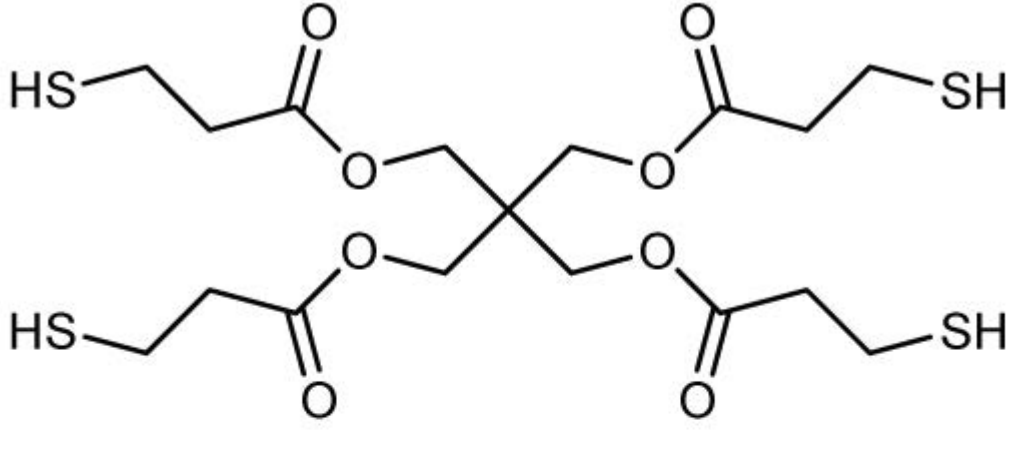

B)

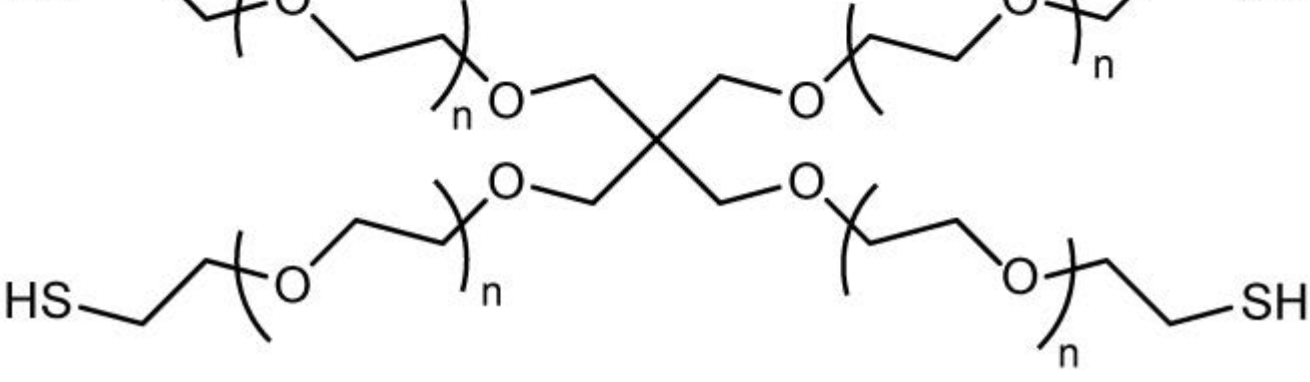

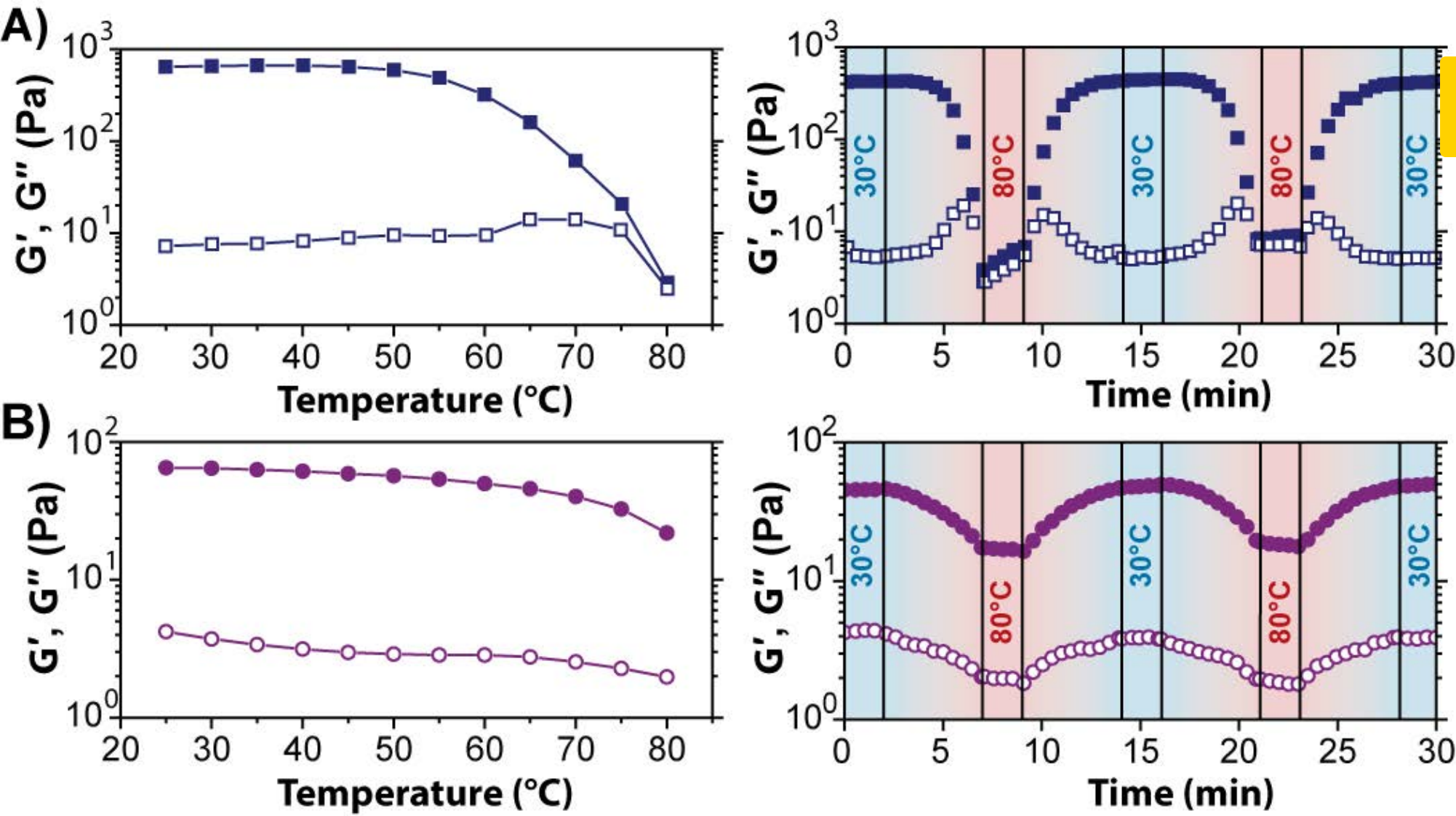
A)
B)
G′, G″ (Pa)
Temperature (°C)
Time (min)
30°C
80°C